forum acusticum 2026
8-12 September · Graz, Austria

COMPUTATIONAL STUDY OF SOUND PRODUCTION IN A FLUE INSTRUMENT USING HELMHOLTZ DECOMPOSITION

N. Giordano[1]

[1] *Department of Physics, Aburn University, Auburn, Alabama, USA*

This paper is a revised version of the authors' submitted manuscript that was peer-reviewed by at least two anonymous reviewers.

Abstract

A direct numerical solution of the Navier-Stokes equations was used to obtain the time dependence of the pressure and air velocity in and around a recorder as it produced a musical tone. A Helmholtz decomposition was then applied to extract the irrotational and solenoidal components of the velocity. The simulations also yielded the Lamb vector, allowing a comparison with predictions for the generation of acoustic energy based on Howe's energy corollary.

Keywords: *recorder, flue instrument, Navier-Stokes-based simulations, Helmholtz decomposition*

1. Introduction

The player of a wind instrument provides a "dc" input of energy via an air jet established by blowing into a mouthpiece. A portion of this energy is converted into oscillations of the air inside the instrument, producing the sound that is emitted, as illustrated very schematically in Fig. 1. Far outside the instrument the velocity field of the air is well-described by the equations of linear acoustics (i.e., sound waves) and is irrotational. However, inside the instrument and especially in the vicinity of the mouthpiece, the air motion is more complicated, containing a combination of irrotational and solenoidal (vorticular) motion. General theoretical treatments (e.g., [1-5]) predict how energy is exchanged between the irrotational and solenoidal components of the velocity field but applying these theoretical expectations in more than a qualitative way to musical instruments has proved to be extremely challenging.

This challenge is also encountered and discussed extensively in studies of aeroacoustics in other contexts (e.g., [6,7]). Many of these discussions begin by assuming that the full (i.e., total) velocity field is separated, at least conceptually, into irrotational and solenoidal components, known as a Helmholtz decomposition. A well-behaved vector field, as expected to be produced by a musical instrument, can be written as the sum of irrotational and solenoidal components which are unique. The irrotational component can be expressed as the gradient of a scalar potential and in the language of acoustics is commonly termed the acoustic velocity [5]. The solenoidal component can be expressed as the curl of a vector potential, and contains the vorticity of the velocity field. This vorticity and the acoustic velocity play central roles in theories of aeroacoustics [1-7].

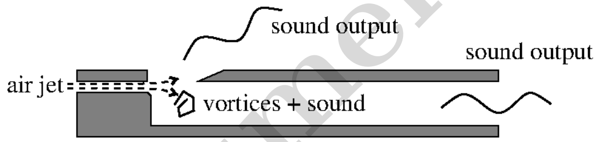

Figure 1: Schematic of a recorder and the qualitative nature of the velocity field in different regions.

There have been several studies of musical instruments that have attempted to separate the irrotational and solenoidal components of the velocity field for a flue instrument. In essentially all cases, those works have made use of either experimental [8,9] or computational [10-12] approaches in which two different blowing excitations are employed. One of these excitations produces the full velocity field (composed of the vorticular and irrotational parts), while the second yields just the irrotational field which is then assumed to be the same as the irrotational motion created with the first blowing excitation. While those studies have yielded interesting results and found general agreement with the theory, it is still of interest to carry out a study that does not rely on this assumpton. That is, a study in which the acoustical field is extracted from the full velocity field obtained from a single blowing condition in which the instrument produces a realistic musical tone.

The work described in this paper uses Navier-Stokes-based simulations of a recorder to investigate the

Corresponding author: *njg0003@auburn.edu.*

velocity field inside and around what is arguably the simplest of wind instruments. We have obtained results for this field with high spatial and time resolution as a musical tone was generated. A Helmholtz decomposition to extract the acoustical velocity from the full velocity field, has been carried out with special attention to the mouthpiece region. The vorticular part of the velocity field has also used to calculate the effective force that, according to Howe's energy corollary, powers the acoustic velocity [3-5]. Comparison of this driving force with the acoustic velocity obtained via decomposition then allows a test of the theory. In the following sections we describe our simulations followed by results for the total velocity field, the vorticity, the Lamb vector, and the acoustic velocity. Much more analysis is needed, so these results should be viewed as an initial progress report.

2. Computational method

A direct numerical solution of the compressible Navier-Stokes equations for a model of a soprano recorder was carried out using an explicit finite difference-time domain algorithm as described in [13,14]. Those references also describe previous results with this computational approach that has found good agreement with experimental results for real recorders. For the model considered in this paper, the mouthpiece was similar to that found in a Yamaha YRS23 instrument while the resonator was a straight cylinder of diameter 13 mm and length of 30 cm without tone holes. As in most real recorders, the channel had a 45° chamfer on the bottom edge. The ratio of the channel-labium distance to the channel height (along the x direction in Fig. 2), was 4.0 as commonly found in soprano recorders. The base note of the instrument is C5 which has a fundamental frequency of approximately 525 Hz. The Navier-Stokes equations yielded the velocity field on a Cartesian grid. Inside and near the outside surfaces of the instrument the grid steps were 0.1 mm in all three dimensions. As explained in [13,14], the instrument was situated in a rectangular box with dimensions $100 \times 60 \times 60$ cm^3 and with weakly absorbing surfaces. The total number of grid points was approximately 1×10^9. In our simulation the speed of the air jet on the central axis of the channel was 8.0 m/s. Starting from quiescent conditions (i.e., without blowing), steady state oscillations of the air velocity and pressure were reached about 100 ms after blowing was initiated. The velocity field in steady state was used in the Helmholtz decomposition analysis. We know from previous work that this blowing speed is large enough to produce a normal musical tone dominated by the spectral component at the frequency associated with C5 (525 Hz), but small enough that the spectral powers at the higher harmonics are smaller by several orders of magnitude or more.

A Helmholtz decomposition was carried out as described by previous authors; see e.g., [6,15]. The scalar potential ϕ was calculated by solving the Poisson equation using a successive over-relaxation algorithm, with

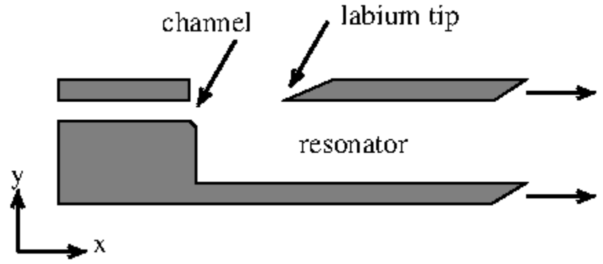

Figure 2: Expanded view of the mouthpiece region. For our computational recorder model, the channel had a rectangular cross-section with a height along y of 1.0 mm and width along z of 13 mm. The distance between the exit of the channel and the tip of the labium was 4.0 mm. Other dimensions are given in the text.

a source term equal to the divergence of the total flow velocity $\boldsymbol{u}$ (bold symbols represent vector quantities)

$$\nabla^2 \phi = \boldsymbol{\nabla} \cdot \boldsymbol{u} \ . \tag{1}$$

The gradient of the scalar potential then yielded the irrotational component of the velocity which we denote by $\boldsymbol{u}_{IR}$; this is also just the acoustic velocity,

$$\boldsymbol{u}_{IR} = \nabla \phi \ . \tag{2}$$

It is known [6,15] that this approach for decomposition yields distorted results in regions near certain sharp corners like those found at the channel exit in Fig. 2. Regions where this distortion is significant are easily identified by visual inspection and are not significant in the results shown below. In the future we plan to carry out the Helmholtz decomposition in a different way, by first estimating the vector potential associated with the solenoidal flow field. As shown in [6] this approach for decomposition is not affected by the distortion encountered with Eq. 1. Unfortunately, a decomposition employing the vector potential is more complicated numerically than dealing with the scalar potential; we plan to explore that approach in the future. Fortunately, we are still able to obtain useful results by dealing only with the scalar potential.

As noted above, our Navier-Stokes computation directly yields the total flow velocity, from which the vorticity $\boldsymbol{\omega}$ can be obtained

$$\boldsymbol{\omega} = \nabla \times \boldsymbol{u} \ . \tag{3}$$

According to Howe [3,5] this vorticular fluid motion acts as a source of sound in the acoustic equations for the (acoustic) velocity $\boldsymbol{u}_{IR}$ with a effective force

$$\boldsymbol{f}_V \sim -\boldsymbol{\omega} \times \boldsymbol{u} \ . \tag{4}$$

which we can also extract from our results, independent from the Helmholtz decomposition. The cross product in Eq. 4 is also termed the Lamb vector. There are important numerical aspects to the analysis with regards to the evaluations involved in Eqs. 1, 3, and 4, and the Poisson solver. These will be discussed in Sec. 4 after some results are described in the next section.

3. Results and discussion

Figure 3 shows an image of the air jet at one instant of an oscillation cycle. Here the jet color is determined by the magnitude of the total flow velocity $\boldsymbol{u}$. Vortices are clearly visible from the general shape of the air jet and as regions where the speed is very small. While the image in Fig. 3 shows only the air speed on the midplane of the instrument and at one particular instant of time, the full velocity field is known in three dimensions both inside and outside the instrument, as is needed to perform the decomposition. In this image and in later figures the coordinate axes are as defined in Fig. 2 with the z direction perpendicular to the plane of the figure. Also note that the images in later Figs. 4, 5, and 6 were recorded at the same instant of time as in Fig. 3.

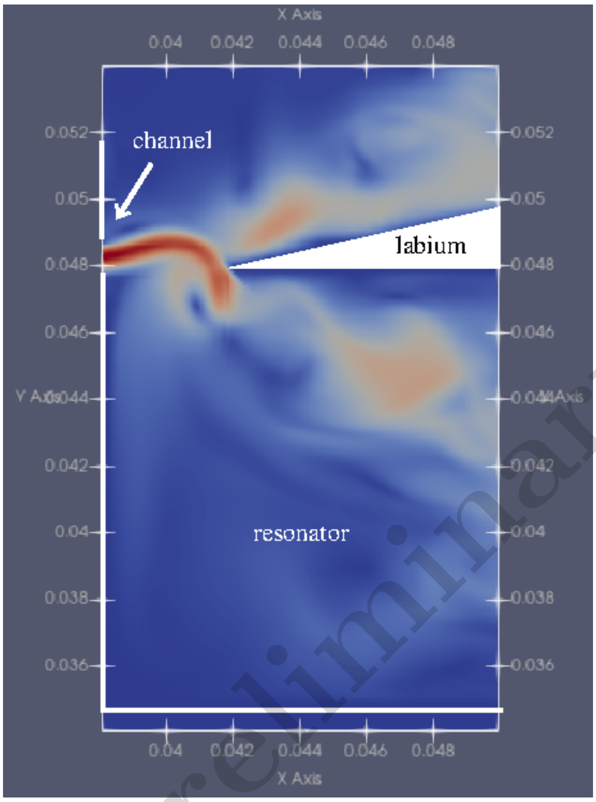

Figure 3: Image of the air jet on the midplane of the instrument as it emerges from the channel and interacts with the labium. The image color shows the magnitude of the velocity, with the darkest red corresponding to 8 m/s and dark blue to a speed of zero. The distance from the channel exit to the labium tip is 4.0 mm. This image shows only the region near the labium as shown roughly in Fig. 2. The bottom edge of the resonator is near the bottom of this image and is shown as the heavy horizontal white line. The $y-z$ edge of the resonator is shown as the heavy vertical white line. The tick marks on all four edges of the image are spaced 2 mm apart.

From the total flow field it is straightforward to find

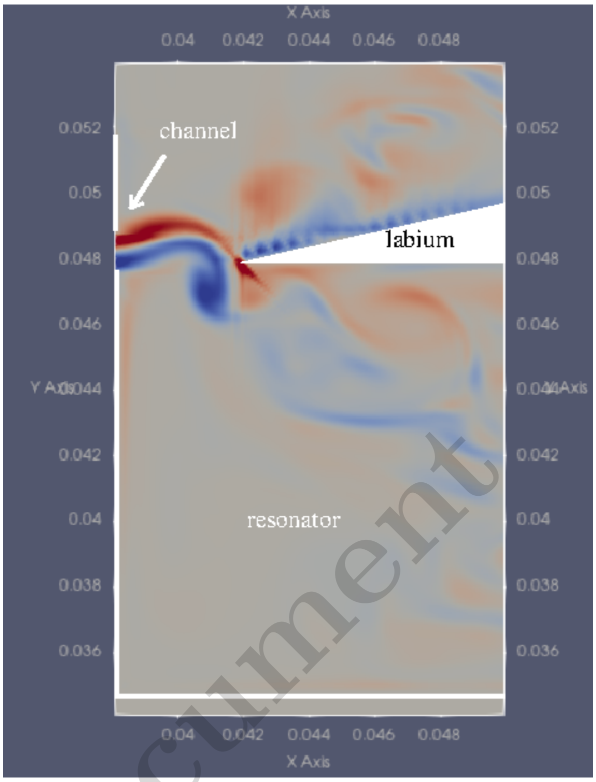

Figure 4: Vorticity in the z direction, perpendicular to the plane of the figure, in the mouthpiece region. This result for the vorticity was obtained at the same instant as image of the flow speed in Fig. 3. The image color shows the value of the vorticity, with the darkest red being $15,000\ \mathrm{s}^{-1}$ and the dark blue corresponding to $-15,000\ \mathrm{s}^{-1}$, and with a positive sign indicating a vorticity vector in the $+z$ direction (see the coordinate system in Fig. 2). The very small dark blue circular regions on the top surface of the labium are due to the way the sloped top edge of the labium projects onto the Cartesian grid used in the calculation. This image shows the same area of the mouthpiece as in Fig. 3, with the edges of the resonator shown as heavy white lines.

the vorticity, Eq. 3. This vorticity is largest along the z direction, and Fig. 4 shows the z component of the vorticity. The divergence of the velocity field (not shown here) is straightforward to calculate; it is used to find the potential ϕ through Eq. 1.

We will also be interested in the force, Eq. 4, which can be found from the vorticity along with the components of the velocity $\boldsymbol{u}$. The component of this force in the x direction is shown in Fig. 5. We note again that this image, like all the others in this paper, is captured at the same time instant as in Fig. 3. From the image in Fig. 5, and from examination of the images at other times during an oscillation cycle, large values of $\boldsymbol{f}_V$ are found near the labium just as the air jet passes and "breaks off" from the tip of the labium. (See also the image of the vorticity in Fig. 4.) Note that we have focused here on the x component of this force since we expect the x component of the acoustic velocity to be largest at the entrance to and inside the resonator.

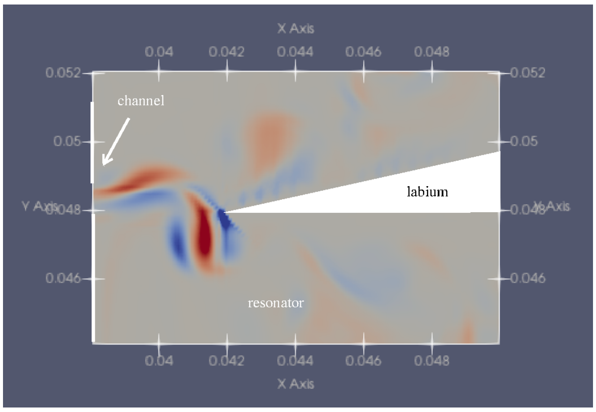

Figure 5: Force $\boldsymbol{f}_V$ (i.e., component of the Lamb vector) in the x direction at the same instant as in Figs. 3 and 4. This image shows an expanded view relative to those in previous figures, with the bottom edge of the resonator now below the bottom of the figure. The scale in this figure can be judged from the distance from the channel exit to the tip of the labium (4.0 mm). The image color shows the value of $\boldsymbol{f}_V$ with the darkest red being 10^5 m/s^{-1} and the dark blue corresponding to -10^5 m/s^{-1}, and with a positive sign indicating $+z$ direction (see the coordinate system in Fig. 2).

Figure 6 shows a result obtained from the Helmholtz decomposition. This image, like all the others shown above, shows the behavior on the midplane of the instrument; i.e., an $x - y$ plane that cuts through the central axis of the instrument. This figure shows the x component of the compressible flow field, i.e., the acoustic velocity, at the same instant as shown in previous figures.

At the instant shown in Fig. 6 the acoustic velocity along x is large in the center of the mouthpiece region, approximately half-way between the exit of the channel and the tip of the labium. This suggests that there is a significant generation of acoustic energy at this point. However, to understand the generation of the acoustic velocity it is necessary to consider the time dependence of $\boldsymbol{u}_{IR}$ at this and other locations in the mouthpiece region as functions of time. In Figure 7 we show the time dependences of the Howe force and the acoustic velocity as functions of time at the point marked by the "X" in Fig. 6. In both of the plots in Fig. 7 we show the x components of each quantity. Both exhibit a complex time depencence, with spectral components at the fundamental frequency of the note C5 (period approximately 2.0 ms) with significant strength at what appear to be harmonics. The fact that the peaks of the Howe force and the acoustic velocity do not occur at the same time is not surprising since the acoustic velocity is a propagating quantity whose value at a particular time and place is due to energy creation at other locations at previous times. The results in Fig. 7 suggest that acoustic energy is created at and near this location of the mouthpiece, but much further analysis is needed

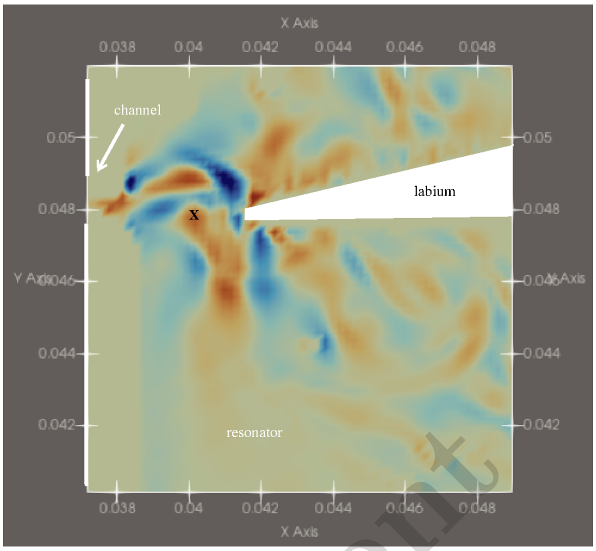

Figure 6: Result for the x (horizontal) component of the scalar potential at the instant considered in Figs. 2, 3, and 4. The edges of the labium and the walls of the channel and resonator are effectively broadened as compared with previous figures due to the fact that the evaluations required in solving for the scalar potential in Eq. 1 involve derivatives that span multiple grid points. The "X" is a location in the mouthpiece region that will be important in the discussion in connection with Fig. 7.

and planned.

4. Present analysis and future directions

As mentioned in the Introduction the results presented in this paper are the result of an initial attempt to implement a Helmholtz decomposition to extract the acoustic velocity from "data" derived from a numerical solution based on the full Navier -Stokes equations for a compressible fluid. To the best of our knowledge this is the first analysis of this kind applied for a wind instrument blown so as to produce a normal musical tone using either computational or experimental data. While Sec. 2 outlined the basic theory that underlies our analysis, in this section some of the important numerical aspects of our analysis are described. We will also discuss plans for further analyses that we hope to pursue in the near future using these data.

Given a flow field, i.e., in our case the air velocity as a function of position throughout the inside of the instrument and in the neighborhood outside, Helmholtz decomposition involves basically two calculations. First, the calculation of the divergence of the velocity to yield $\nabla^2\phi$ through Eq. 1, and second, solving the resulting Poisson equation to yield ϕ. Both of these steps contribute to the numerical accuracy of the final result for the acoustic velocity through Eq. 2. In the present work, the divergence of the velocity was determined by differentiating $\boldsymbol{u}$ which was known on a three dimensional Cartesian grid with spacing $\Delta = 0.1$ mm in all three dimensions. To reduce the

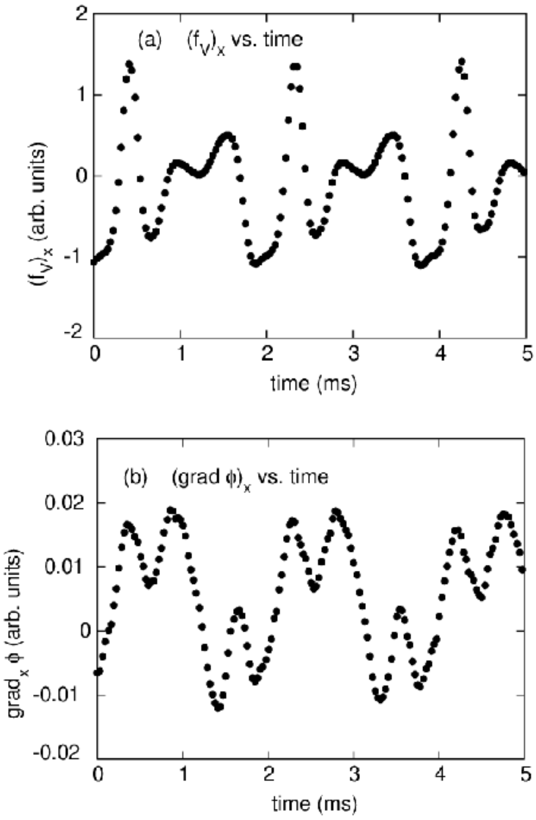

Figure 7: Result for time dependences of (a) the x (horizontal) component of the Howe force (Eq. 4) and (b) the x component of the irrotational flow velocity, i.e., the acoustic velocity (Eq. 2) at a point near the center of the window region.

effect of finite grid size the results for $\boldsymbol{u}$ were averaged over cubical cells of size $2 \times 2 \times 2\ \Delta^3$. Results were also obtained with other cell sizes, and it was judged that this choice of cell size for spacial averaging was a satisfactory compromise for obtaining good spatial resolution together with adequate averaging. In order to judge the uncertainties in the divergence computed with these cell averaged values, we compared results with the divergence computed to third and fifth order in the step size and found that the results differed very little in going from third to fifth order. The resulting Poisson equation was solved to second order using a standard simultaneous over relaxation algorithm, with hard wall boundary conditions. Hence numerically, the final results are accurate only to second order. One of our plans for the future is to implement a fourth order Poisson solver. Note that this decomposition was performed for each time step in the overall calculation. This time step was 3.1×10^{-5} s, giving a resolution in time of approximately 0.015 of the acoustic period.

Another limitation of the numerical accuracy of our final results was due to the acute interior angles in the recorder geometry found at the exit of the channel. As discussed in [6] the singularities at these corners produce the distortions in the final result for ϕ. Fortunately, this distortion does not appear to be a problem in the regions in the mouthpiece that are of greatest interest for our purposes, and which yielded the results in Figs. 6 and 7. For the future we plan to explore algorithms that can overcome these difficulties, including performing the decomposition via the vector potential. That is a problem that we leave for the future.

One final note should be made concerning the results in Figs. 5, 6, and 7. In those figures we considered only the components of the Howe force $\boldsymbol{f}_V$ and $\boldsymbol{u}_{IR}$ along the x direction. Both of these quantites have significant values along y, especially in the region between the channel exit and the labium tip (see [11]). We plan to study in detail the full behavior of these quantities along both the x and y directions and away from the midplane of the instrument, and will report those results in the near future.

5. Conclusions and outlook

This paper describes a successful Helmholtz decomposition analysis of the velocity field in a wind instrument while it is sounding a realistic musical tone. We have shown that it is possible to extract considerable quantitative information relating to the time and space dependencies of the vorticity and other aeroacoustic quantities from Navier-Stokes-based simulations. Our results give a qualitative picture of how motion of the air jet and its interaction with the labium creates acoustic energy during the course of its oscillation in the window region. Further quantitative analysis of these results is now in progress.

Acknowledgments

The author thanks K. L. Saenger for useful discussions. This research was supported by the US National Science Foundation through grant PHY-2306035, and used computational facilities at Auburn University and Purdue University.

References

1. M. J. Lighthill, "On sound generated aerodynamically, I. General theory," Proc. R. Soc. London **211**, 564-587 (1952).

2. M. J. Lighthill, "On sound generated aerodynamically, II. Turbulence as a source of sound," Proc. R. Soc. London **222**, 1-31 (1954).

3. M. S. Howe, "The dissipation of sound at an edge," J. Sound and Vib. **70**, 407-411 (1980).

4. A. Powell, "Some aspects of aeroacoustics: From Rayleigh until today," J. Vib. and Acoustics **112**, 144-159 (1990).

5. A. Hirschberg, "Introduction to aeroacoustics of internal flows," in Advances in Aeroacoustics, Von Karman Institute for Fluid Dynamics, 112 pp (2007).

6. S. Schoder, K. Roppert, and M. Kaltenbacher, "Helmholtz's decomposition for compressible flows and its application to computational aeroacoustics," SN Partial Differ. Equ. Appl. **1:46**, 20 pp (2020).
7. R. Ewert and J. Kreuzinger, "Hydrodynamic/acoustic splitting approach with flow-acoustic feedback for universal subsonic noise computation," J. Comp. Physics **444**, 110548 (2021).
8. A. Bamberger, "Vortex sound in flutes using flow determination with Endo-PIV," Proceedings of the International Congress on Acoustics 2004, Vol. II, 1417-1420. (2004).
9. S. Yoshikawa, H. Tashiro, and Y. Sakamoto, "Experimental examination of vortex-sound generation in an organ pipe: A proposal of jet vortex-layer formation model," J. Sound and Vib. **331**, 2558-2577 (2012).
10. H. Kühnelt, "Vortex sound in recorder- and flute-like instruments: Numerical simulation and analysis," Proceedings of the International Symposium on Musical Acoustics, Barcelona, Spain, 5 pp (2007).
11. H. Kühnelt, "Studying the vortex sound of recorder- and flute-like instruments by means of the lattice Boltzmann method and Helmholtz decomposition," Ph.D. thesis, Universität fur Musik und Darstellende Kunst Wein (2016).
12. R. Tabata, R. Matsuda, T. Koiwaya, S. Iwagami, H. Midorikawa, T. Kobayashi and K. Takahashi, "Three-dimensional numerical analysis of acoustic energy absorption and generation in an air-jet instrument based on Howe's energy corollary," J. Acoust Soc. Amer. **149**, 4000-4012 (2021).
13. N. Giordano and K. L. Saenger, "Study of 'half-integer' harmonics in recorder tones and some speculations about their origin," J. Acoust. Soc. Amer. **154**, 2917-2927 (2023).
14. N. Giordano, "Understanding end corrections and flow near the open end of a flue instrument," J. Acoust. Soc. Amer. **157**, 1176-1184 (2025).
15. S. Schoder and M. Kaltenbacher, "Hybrid aeroacoustic computations: State of the art and new achievements," J. Theor. and Comp. Acoustics **27**, 1950020, 33 pp (2019).